ELSEVIER

www.elsevier.nl/locate/jorganchem

Journal of Organometallic Chemistry 582 (1999) 310–318

Journal of Organometallic Chemistry

Mixed-metal cluster chemistry Part 14: reaction of $[Cp_2W_2Ir_2(CO)_{10}]$ with trimethylphosphite; X-ray crystal structures of $[Cp_2W_2Ir_2(\mu\text{-}CO)_3(CO)_5\{P(OMe)_3\}_2]$ and two modifications of $[CpWIr_3(\mu\text{-}CO)_3(CO)_7\{P(OMe)_3\}]$☆

Susan M. Waterman [a], Mark G. Humphrey [a,*], David C.R. Hockless [b]

[a] *Department of Chemistry, Australian National University, Canberra, ACT 0200, Australia*
[b] *Research School of Chemistry, Australian National University, Canberra, ACT 0200, Australia*

Received 23 December 1998

Abstract

Reactions of $[Cp_2W_2Ir_2(CO)_{10}]$ with stoichiometric amounts of trimethylphosphite afford the substitution products $[Cp_2W_2Ir_2(\mu\text{-}CO)_3(CO)_{7-n}\{P(OMe)_3\}_n]$ [$n = 1$ (**2**) or 2 (**3**)]. A structural study of **3** reveals that the three edges of a WIr_2 face of the tetrahedral core are spanned by bridging carbonyls, and that the iridium-bound $P(OMe)_3$ groups ligate radially and axially with respect to the plane of bridging carbonyls. The tungsten-bound η^5-cyclopentadienyl groups ligate axially and apically with respect to the plane of bridging carbonyls. An unusual decomposition reaction was observed during the crystallization of **3**. A single-crystal X-ray study from the second type of crystals from a solution of **3** was identified as the previously synthesized $[CpWIr_3(\mu\text{-}CO)_3(CO)_7\{P(OMe)_3\}]$ (**4**). A structural study of **4** reveals that the cluster core has a WIr_3 tetrahedral framework, with three edges of a WIr_2 face spanned by bridging carbonyls and that the iridium-bound $P(OMe)_3$ and the tungsten-bound η^5-cyclopentadienyl moieties ligate diaxially with respect to the plane of bridging carbonyls. Monitoring a solution of **3** by ^{31}P-NMR spectroscopy reveals slow formation of **4** (93% **3**: 7% **4** over 4 days) at room temperature. One configuration only of clusters **2** and **3** was observed in the ^{13}C- and ^{31}P-NMR spectra (between 183 and 303 K), with no evidence for the presence of additional isomers undergoing very fast exchange. The NMR spectra of **3** are consistent with the formulation given in the X-ray crystallographic study. The NMR spectra of **2** suggest a configuration with axial phosphite, axial Cp, apical Cp, analogous to the related clusters $[Cp_2M_2Ir_2(\mu\text{-}CO)_3(CO)_6(PMe_3)]$ (M = Mo, W), the molybdenum analogue of which has been structurally characterized previously.

Keywords: Tungsten; Iridium; Carbonyl; Phosphite; Cluster

1. Introduction

The chemistry of mixed-metal clusters continues to be of interest [2], with many reports focusing on ligand substitution. Comparative studies of clusters with systematically varied cores are of particular interest. The clusters $[Cp_2W_2Ir_2(CO)_{10}]$ (**1**), $[CpWIr_3(CO)_{11}]$ and $[Ir_4(CO)_{12}]$ comprise a set of three isostructural clusters related by sequential, conceptual replacement of cluster core vertices. Derivatives of these clusters can possess a plane of bridging carbonyls and, with respect to the plane of bridging carbonyls, ligands can be radially, axially or apically disposed (see Fig. 1). The chemistry of $[Ir_4(CO)_{12}]$ with phosphites has been described previously [3–5], with $[Ir_4(CO)_{11}\{P(OPh)_3\}]$ proposed to have an axially ligating phosphite on the basis of IR spectroscopy [3]. A kinetic study of $[Ir_4(CO)_{11}(L)]$ [L = $P(OPh)_3$, $P(OPh)_3$ or $P(OCH_2)_3CEt$], and a structural study of $[Ir_4(CO)_{11}\{P(OCH_2)_3CEt\}]$ (which revealed an all-terminal carbonyl geometry), suggested that these clusters exist as mixtures of interconverting isomers in solution possessing the all-terminal ligand geometry (L = $P(OMe)_3$, $P(OPh)_3$ or $P(OCH_2)_3CEt$) or an edge-

☆ For Part 13 see Ref. [1].

* Corresponding author. Tel.: +62-2-6249-2927; fax: +61-2-6249-0760.

E-mail address: mark.humphreys@anu.edu.au (M.G. Humphrey)

0022-328X/99/$ - see front matter
PII: S0022-328X(99)00075-3

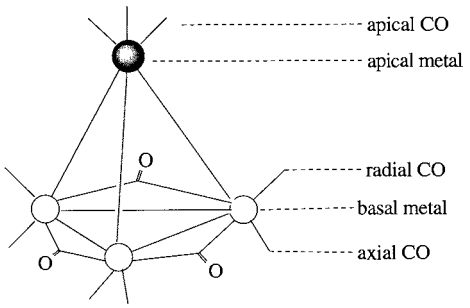

Fig. 1.

bridged structure with the phosphite occupying radial (L = $P(OMe)_3$, $P(OCH_2)_3CEt$ only) or axial sites (L = $P(OMe)_3$, $P(OPh)_3$ or $P(OCH_2)_3CEt$) [4]. The cluster $[Ir_4(CO)_8\{P(OMe)_3\}_4]$ has been proposed to adopt an unusual triaxial, apical geometry [5].

We have recently reported the phosphite reaction chemistry of $[CpWIr_3(CO)_{11}]$ [6]. Some of the products of the reactions, namely $[CpWIr_3(\mu\text{-}CO)_3(CO)_{8-n}(L)_n]$ (L = $P(OMe)_3$, $n = 1$ or 3; L = $P(OPh)_3$, $n = 1$ or 3), exhibit ligand fluxionality in solution, resolvable at low temperatures into the constituent isomers. We have therefore been prompted to investigate the reactions of **1**, the third cluster in the series, with trimethylphosphite. We herein report the results of these reactions, the characterization by single-crystal X-ray study of $[Cp_2W_2Ir_2(\mu\text{-}CO)_3(CO)_5\{P(OMe)_3\}_2]$, as well as structural studies of the previously synthesized $[CpWIr_3(\mu\text{-}CO)_3(CO)_7\{P(OMe)_3\}]$, identification of the geometries of the ditungsten–diiridium clusters by NMR studies, and ligand fluxionality studies of the new phosphite derivatives.

2. Results and discussion

2.1. Syntheses and characterization of $[Cp_2W_2Ir_2(\mu\text{-}CO)_3(CO)_{7-n}\{P(OMe)_3\}_n]$ ($n = 1$ (**2**), 2 (**3**))

The reactions of $[Cp_2W_2Ir_2(CO)_{10}]$ (**1**) with n equivalents of $P(OMe)_3$ ($n = 1$ or 2) proceed in dichloromethane at room temperature (r.t.) to afford the clusters $[Cp_2W_2Ir_2(\mu\text{-}CO)_3(CO)_{7-n}\{P(OMe)_3\}_n]$ ($n = 1$, **2**; $n = 2$, **3**) as the major or sole reaction products in excellent yields (54–76%). The products have been characterized by a combination of IR, ^{1}H-, ^{13}C- and ^{31}P-NMR spectroscopies, MS and satisfactory microanalyses. IR spectra suggest the presence of edge-bridging carbonyl ligands in both complexes (ν(CO) 1869–1807 cm^{-1}), in contrast to the all-terminal precursor **1**. The number of bands in the carbonyl ligand ν(CO) region for clusters **2** and **3** are consistent with the presence of one configuration only, for each cluster, in contrast to most of the previously studied ligand-substituted tungsten–iridium clusters which have IR spectra suggestive of more than one configuration in solution [1,6–10]. The ^{1}H-NMR spectra contain signals assigned to Cp and Me groups in the expected ratios. The FAB mass spectra of the complexes do not contain molecular ions; instead, $[M-2CO]^+$ is the largest fragment observed. These ions fragment by stepwise loss of carbonyls, with particularly intense $[M-3CO]^+$ ions. The isotope patterns are consistent with the presence of two iridium atoms and two tungsten atoms.

2.2. X-ray structural studies of crystals grown from a solution of **3**

Crystallization of a dichloromethane/octane solution of **3** by slow evaporation affords three different types of crystals suitable for X-ray diffraction studies which are separable by hand. An X-ray study of the red, prismatic crystals confirmed the molecular composition of **3**. Two single-crystal X-ray studies of pale orange, plate-like crystals revealed that **3** slowly decomposes in solution to afford $[CpWIr_3(\mu\text{-}CO)_3(CO)_7\{P(OMe)_3\}]$ (**4**).

The single-crystal X-ray study of **3** is consistent with the formulation given above, defines the substitution sites of the phosphites and the η^5-cyclopentadienyl ligands, and aids interpretation of the ^{13}C- and ^{31}P-NMR spectra (see below). A summary of crystal and refinement data is shown in Table 1, and selected bond

Table 1
Crystallographic data for **3**, **4a** and **4b**

	3	**4a**	**4b**
Formula	$C_{24}H_{28}Ir_2O_{14}P_2W_2$	$C_{18}H_{14}Ir_3O_{13}PW$	$C_{18}H_{14}Ir_3O_{13}PW$
Formula weight	1354.56	1229.78	1229.78
Space group	$C2/c$ (no. 15)	$P\bar{1}$ (no. 2)	$P\bar{1}$ (no. 2)
Crystal system	Monoclinic	Triclinic	Triclinic
a (Å)	18.712(3)	8.844(2)	9.497(4)
b (Å)	11.078(5)	10.088(2)	10.021(4)
c (Å)	30.455(3)	15.668(2)	15.986(3)
α (°)		81.85(1)	76.07(2)
β (°)	93.66(1)	78.71(1)	79.32(2)
γ (°)		70.60(2)	62.82(3)
V (Å^3)	6300(3)	1288.6(4)	1308.5(8)
$D_{calc.}$ (g cm^{-3})	2.856	3.169	3.121
Z	8	2	2
μ (mm^{-1})	15.9	37.8	19.7
Specimen size (mm^3)	$0.38 \times 0.32 \times 0.24$	$0.32 \times 0.24 \times 0.04$	$0.36 \times 0.16 \times 0.16$
A (min, max)	0.89–1.00	0.41–1.00	0.21–1.00
$2\theta_{max}$ (°)	50.1	120.0	50.1
N	5894	3820	4618
N_o	4265	3547	3795
R	0.036	0.038	0.032
R_w	0.043	0.050	0.037

Table 2
Selected bond lengths (Å) and angles (°) for $[Cp_2W_2Ir_2(\mu\text{-}CO)_3(CO)_5\{P(OMe)_3\}_2]$ (**3**)

Bond lengths			
Ir(1)–Ir(2)	2.7108(8)	Ir(1)–W(3)	2.8722(9)
Ir(1)–W(4)	2.8885(9)	Ir(2)–W(3)	2.8167(8)
Ir(2)–W(4)	2.8607(8)	W(3)–W(4)	3.0702(9)
Ir(1)–P(1)	2.241(4)	Ir(2)–P(2)	2.250(4)
Ir(1)–C(11)	1.90(2)	Ir(1)–C(12)	2.11(1)
Ir(1)–C(13)	2.16(1)	Ir(2)–C(12)	2.06(2)
Ir(2)–C(21)	1.85(2)	Ir(2)–C(23)	2.12(2)
W(3)–C(13)	2.11(2)	W(3)–C(23)	2.13(2)
W(3)–C(31)	1.93(2)	W(3)–C(301)	2.32(2)
W(3)–C(302)	2.30(2)	W(3)–C(303)	2.30(1)
W(3)–C(304)	2.32(1)	W(3)–C(305)	2.34(1)
W(4)–C(41)	1.98(2)	W(4)–C(42)	2.02(2)
W(4)–C(401)	2.30(1)	W(4)–C(402)	2.35(2)
W(4)–C(403)	2.36(2)	W(4)–C(404)	2.31(1)
W(4)–C(405)	2.28(1)		
Bond angles			
Ir(2)–Ir(1)–W(3)	60.52(2)	Ir(2)–Ir(1)–W(4)	61.35(2)
W(3)–Ir(1)–W(4)	64.41(2)	Ir(1)–Ir(2)–W(3)	62.58(2)
Ir(1)–Ir(2)–W(4)	62.39(2)	W(3)–Ir(2)–W(4)	65.47(2)
Ir(1)–W(3)–Ir(2)	56.90(2)	Ir(1)–W(3)–W(4)	58.05(2)
Ir(2)–W(3)–W(4)	57.96(2)	Ir(1)–W(4)–Ir(2)	56.26(2)
Ir(1)–W(4)–W(3)	57.54(2)	Ir(2)–W(4)–W(3)	56.57(2)
Ir(2)–Ir(1)–P(1)	108.6(1)	W(3)–Ir(1)–P(1)	103.8(1)
W(4)–Ir(1)–P(1)	166.9(1)	Ir(1)–Ir(2)–P(2)	137.6(1)
W(3)–Ir(2)–P(2)	148.1(1)	W(4)–Ir(2)–P(2)	99.7(1)

lengths and angles are shown in Table 2. Fig. 2 contains an ORTEP plot of **3** showing the molecular geometry and atomic numbering scheme.

Complex **3** has the pseudotetrahedral framework of the precursor cluster **1**. Each tungsten atom bears one η^5-cyclopentadienyl group; three bridging carbonyls span a WIr_2 face, and five terminal carbonyl ligands and two iridium-ligated trimethylphosphite ligands complete the coordination sphere. The W_2Ir_2 core distances ($W–Ir_{av} = 2.86$ Å, $W–W = 3.0702(9)$ Å) are slightly longer than those of **1** [11] ($W–Ir_{av}$ 2.835, W–W 2.991(1)) while the Ir–Ir distance (2.7108(8) Å for **3** compared with 2.722(1) Å for **1**) is marginally shorter, consistent with a core expansion on introduction of phosphite; core distances of the related mono(phosphine)-substituted cluster $[Cp_2W_2Ir_2(\mu\text{-}CO)_3(CO)_6(PPh_3)]$ [1] are also consistent with core expansion upon introduction of a *P*-donor ligand. The longest W–Ir core distance for **3** is effectively *trans* to both the apical Cp group and the axially ligating $P(OMe)_3$. Ir–CO(terminal) interactions for **3** (1.85(2), 1.90(2) Å) and Ir–C–O(terminal) angles (176(2), 177(2)°) are unexceptional. Intracore bond angles are all close to 60°, as expected. As was observed with **1**, and the related $[Cp_2W_2Ir_2(\mu\text{-}CO)_3(CO)_6(PPh_3)]$, angles centred at iridium for **3** (60.52(2)–65.47(2)°) are slightly larger than those centred at tungsten (56.90(2)–58.05(2)°). The Ir–P distances (2.250(4), 2.241(4) Å) are, as expected, slightly shorter than those in the previously reported phosphine-substituted ditungsten–diiridium cluster (2.348(3) Å) [1]. Intraphosphite bond lengths and angles are not unusual. With respect to the plane of bridging carbonyls, the $P(OMe)_3$ ligands occupy radial and axial coordination sites with the cyclopentadienyl groups in axial and apical positions. This radial, diaxial, apical disposition of ligands in **3** has not been structurally identified previously with tungsten–iridium clusters, but it is the tetra-substituted configuration which is predicted to be of lowest energy on steric grounds (the apical ligand is inclined to the face containing the two axial ligands).

The formation of crystals of **4**, grown from a solution of **3**, reveals that the ditungsten–diiridium cluster framework of **3** slowly decomposes in solution at r.t. to afford the tungsten–triiridium framework of cluster **4**. A structural study of one crystal of **4** at 183 K (crystal modification **4a**) was observed to have a different unit cell and slightly different bond length and angle parameters from that of a structural study of a second crystal of **4** at 298 K (crystal modification **4b**). A unit cell determination of the second crystal of **4** at 183 K revealed that the cell parameters were temperature invariant and that no structural modifications to the crystals of **4** were occurring on raising or lowering the temperature. The present work has therefore afforded an unusual instance of two crystal modifications of a cluster from the same solvent mixture. The single-crystal X-ray studies of **4a** and **4b** confirm that the decom-

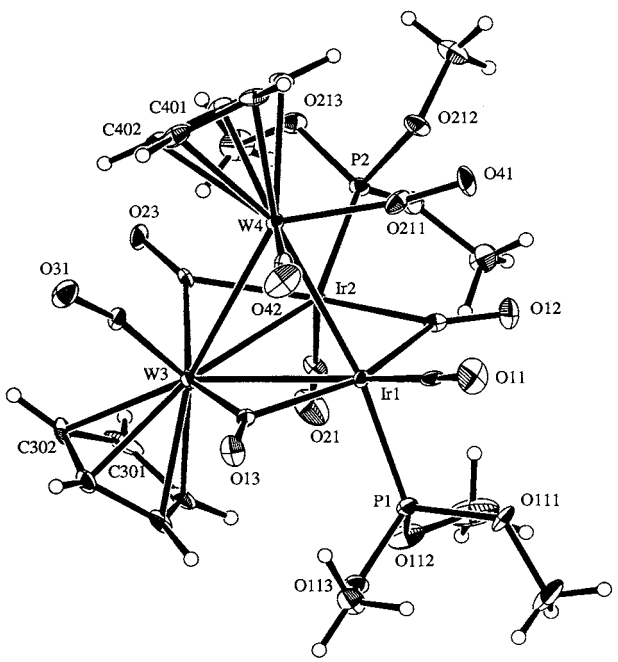

Fig. 2. Molecular structure and atomic labelling scheme for $[Cp_2W_2Ir_2(\mu\text{-}CO)_3(CO)_5\{P(OMe)_3\}_2]$ (**3**). 20% thermal envelopes are shown for the non-hydrogen atoms; hydrogen atoms have arbitrary radii of 0.1 Å.

Table 3
Selected bond lengths (Å) and angles (°) for $[CpWIr_3(\mu\text{-}CO)_3(CO)_7\{P(OMe)_3\}]$ (**4a** and **4b**)

	4a	4b
Bond lengths		
Ir(1)–Ir(2)	2.6885(8)	2.7005(9)
Ir(1)–Ir(3)	2.7453(7)	2.7196(6)
Ir(2)–Ir(3)	2.7148(8)	2.717(1)
Ir(1)–W(1/4)	2.8640(7)	2.8699(6)
Ir(2)–W(1/4)	2.8470(7)	2.8167(6)
Ir(3)–W(1/4)	2.9043(8)	2.9020(7)
Ir(1)–P(1)	2.251(3)	2.247(3)
Ir(1)–C(1)	2.08(1)	2.10(1)
Ir(1)–C(3)	2.13(1)	2.10(1)
Ir(1)–C(11)	1.87(1)	1.86(1)
Ir(2)–C(1)	2.12(1)	2.14(1)
Ir(2)–C(2)	2.19(1)	2.22(1)
Ir(2)–C(21)	1.90(1)	1.88(2)
Ir(2)–C(22)	1.90(2)	1.88(1)
Ir(3)–C(31)	1.87(2)	1.89(2)
Ir(3)–C(32)	1.94(2)	1.93(2)
Ir(3)–C(33)	1.94(2)	1.91(1)
W(1/4)–C(01)	2.31(1)	2.33(1)
W(1/4)–C(02)	2.27(1)	2.32(1)
W(1/4)–C(03)	2.33(1)	2.30(1)
W(1/4)–C(04)	2.32(1)	2.31(1)
W(1/4)–C(05)	2.36(1)	2.33(1)
W(1/4)–C(2)	2.11(1)	2.13(1)
W(1/4)–C(3)	2.15(1)	2.14(1)
W(1/4)–C(41)	1.98(1)	1.97(1)
Bond angles		
Ir(2)–Ir(1)–Ir(3)	59.94(2)	60.16(2)
Ir(2)–Ir(1)–W(1/4)	61.60(2)	60.66(2)
Ir(3)–Ir(1)–W(1/4)	62.32(2)	62.49(2)
Ir(3)–Ir(2)–W(1/4)	62.91(2)	63.23(2)
Ir(1)–Ir(2)–Ir(3)	61.07(2)	60.27(3)
Ir(1)–Ir(2)–W(1/4)	62.23(2)	62.65(2)
Ir(1)–Ir(3)–Ir(2)	58.99(2)	59.57(2)
Ir(1)–Ir(3)–W(1/4)	60.84(2)	61.29(2)
Ir(2)–Ir(3)–W(1/4)	60.77(2)	60.07(2)
Ir(1)–W(1/4)–Ir(2)	56.17(2)	56.70(2)
Ir(1)–W(1/4)–Ir(3)	56.84(2)	56.22(2)
Ir(2)–W(1/4)–Ir(3)	56.32(2)	56.70(2)
Ir(2)–Ir(1)–P(1)	106.34(9)	109.12(8)
Ir(3)–Ir(1)–P(1)	162.55(9)	166.20(8)
W(1/4)–Ir(1)–P(1)	102.41(8)	105.29(8)

position product of **3** is the previously reported cluster $[CpWIr_3(\mu\text{-}CO)_3(CO)_7\{P(OMe)_3\}]$ (prepared in earlier work by reaction of $[CpWIr_3(CO)_{11}]$ with one equivalent of $P(OMe)_3$ [6]); the present structural study defines the substitution sites of the phosphite and the η^5-cyclopentadienyl ligand. Crystal and refinement data are shown in Table 1, and selected bond lengths and angles are listed in Table 3. Fig. 3 contains an ORTEP plot showing the molecular geometry and atomic numbering scheme.

Complex **4** has the pseudotetrahedral framework of the related cluster $[CpWIr_3(CO)_{11}]$ [12], and possesses an η^5-cyclopentadienyl group, three bridging carbonyls arranged around a WIr_2 plane, seven terminal carbonyls, and an iridium-ligated trimethylphosphite ligand. The WIr_3 core distances ($W–Ir_{av} = 2.87$ Å **4a**, 2.86 Å **4b**; $Ir–Ir_{av} = 2.72$ Å **4a**, 2.71 Å **4b**) are slightly longer than those of $[CpWIr_3(CO)_{11}]$ ($W–Ir_{av} = 2.82$ Å **4**; $Ir–Ir_{av} = 2.70$ Å [12]); core distances of the related monophosphine substituted clusters $[CpWIr_3(\mu\text{-}CO)_3(CO)_7(PPh_3)]$ [10], $[CpWIr_3(\mu\text{-}CO)_3(CO)_7(PMe_3)]$ [10] and $[CpWIr_3(\mu\text{-}CO)_3(CO)_7(PMe_2Ph)]$ [9] are also consistent with core expansion upon introduction of a *P*-donor ligand. The longest W–Ir core distance for **4a** and **4b** is effectively *trans* to the Cp group. Ir–CO(terminal) interactions (1.87(1)–1.94(2) Å **4a**; 1.86(1)–1.93(2) Å **4b**) and W–CO(terminal) interactions (1.98(1) Å **4a**, 1.97(1) Å **4b**) are unexceptional. As with **3**, the Ir–P distances (2.251(3) Å **4a**, 2.247(3) Å **4b**) are comparable to those of the phosphite-containing cluster $[CpWIr_3(\mu\text{-}CO)_3(CO)_6\{P(OPh)_3\}_2]$ (2.230(3), 2.239(3) Å) [6], and slightly shorter than those in the previously reported phosphine-substituted tungsten–triiridium clusters (2.312(7)–2.34(1) Å) [9,10]. Intraphosphite bond lengths and angles are not unusual. The diaxial disposition of ligands in **4a** and **4b** has not been structurally identified previously in the tungsten–iridium cluster system. Formal electron counting reveals that the clusters **3**, **4a** and **4b** have 60 electrons, electron precise for tetrahedral clusters.

Cluster **4** has previously been postulated to exist as a mixture of two isomers (axial phosphite, apical Cp; axial phosphite, radial Cp) [6]. Although two structurally characterized examples of ligand-substituted tungsten–iridium clusters with axial, apical coordination geometries are extant [9,10], crystallographically characterized examples of clusters with radial η^5-cy-

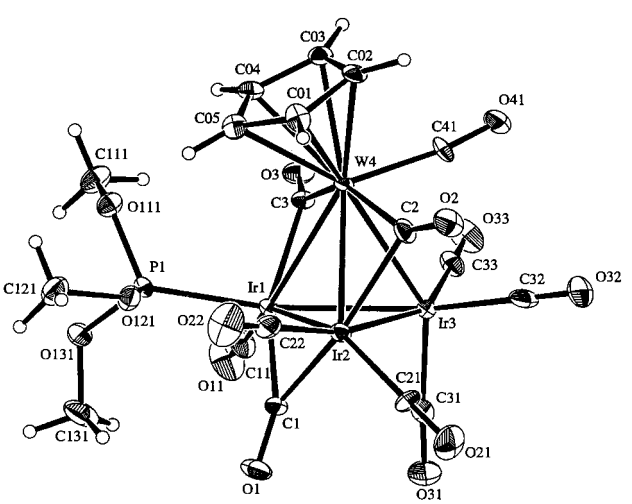

Fig. 3. Molecular structure and atomic labelling scheme for $[CpWIr_3(\mu\text{-}CO)_3(CO)_7\{P(OMe)_3\}]$ (**4a** and **4b**). 20% thermal envelopes are shown for the non-hydrogen atoms; hydrogen atoms have arbitrary radii of 0.1 Å.

clopentadienyl ligands have thus far proven elusive. The axial, radial coordination geometry has been proposed for isomers of $[CpWIr_3(\mu\text{-}CO)_3(CO)_7(PPh_3)]$ [8] and $[CpWIr_3(\mu\text{-}CO)_3(CO)_7\{P(OPh)_3\}]$ [6] to minimize phosphine/phosphite–cyclopentadienyl repulsion. The diaxial coordination geometry of **4** is favourable only because of the small cone angle nature of the $P(OMe)_3$ ligand. Diaxial coordination geometries are unusual in the homometallic system, with $[Ir_4(H)_2(\mu\text{-}CO)_3(CO)_7]^{2-}$ [13], $[Ir_4(\mu\text{-}CO)_3(CO)_7(\overline{COCH_2CH_2O})_2]$ [14], and $[Ir_4(\mu\text{-}CO)_3(CO)_7(CH_2CO_2Me)_2]^{2-}$ [15] crystallographically confirmed in the 'parent' tetrairidium system and $[Co_4(\mu\text{-}CO)_3(CO)_7\{P(OMe)_3\}_2]$ [16] structurally characterized in the related tetracobalt system (in each case, the cone angle of the entering ligand is small). Amongst heterometallic clusters, diaxial coordination geometries have been crystallographically confirmed for $[FeCo_3(\mu_3\text{-}H)(\mu\text{-}CO)_3(CO)_7(PPh_3)_2]$ [17], $[RuCo_3(\mu_3\text{-}H)(\mu\text{-}CO)_3(CO)_7(PPh_3)_2]$ [18], $[RuRh_3(\mu_3\text{-}H)(\mu\text{-}CO)_3(CO)_7(PPh_3)_2]$ [18], and $[RuCoRh_2(\mu_3\text{-}H)(\mu\text{-}CO)_3(CO)_7(PPh_3)_2]$ [19], but in all cases a face-capping hydride lies below the basal plane; this has been reported to cause the radial carbonyls to be displaced towards the apical metal, providing more room for the incoming ligand in axial sites than in radial sites.

2.3. Decomposition of 3 to 4 by ^{31}P-NMR spectroscopy

A $^{31}P\{^1H\}$-NMR spectroscopic study of **3** in CD_2Cl_2 at 298 K was undertaken to monitor its decomposition into $[CpWIr_3(\mu\text{-}CO)_3(CO)_7\{P(OMe)_3\}]$ (**4**) in solution. ^{31}P-NMR spectra of **3** were measured every 2 h over a 72 h period. The ^{31}P-NMR spectrum at 0 h reveals two signals at 123.5 and 99.5 ppm, corresponding to the radial and axial phosphites of **3** (see Section 2.4). After 12 h, a small signal at 87.1 ppm appears followed, after 72 h, by a very minor signal at 98.5 ppm. A ^{31}P-NMR spectrum of pure **4** in CD_2Cl_2 at 298 K under the same experimental conditions reveals a signal at 87.1 ppm, and the corresponding signal from the decomposition study is therefore assigned to $[CpWIr_3(\mu\text{-}CO)_3(CO)_7\{P(OMe)_3\}]$ (**4**). Cluster **4** is known to be fluxional on the NMR timescale [6], but an attempt to resolve the constituent isomers of **4** by lowering the temperature to 178 K was unsuccessful due to the low concentration of **4** in solution. The minor signal at 98.5 ppm may possibly correspond to **2**, another possible decomposition product, although the concentration is too low for this to be confirmed. After 72 h, the ^{31}P-NMR spectrum of **3** shows that the relative abundance of the components is (**3**) 92:(**4**) 7:(**2**) 1. Although the sample of **3** was left in solution for a further 28 days, ^{31}P-NMR spectroscopy did not reveal significant additional conversion of **4** to **3**.

Decomposition-induced modifications to the coordination sphere have been noted before in ligand-substituted tungsten–iridium clusters. The sterically-encumbered clusters $[CpWIr_3(\mu\text{-}CO)_3(CO)_5(PPh_3)_3]$ [8,10] and $[Cp_2W_2Ir_2(\mu\text{-}CO)_3(CO)_5(PPh_3)_2]$ [1] decompose rapidly in solution at r.t. or on a preparative thin-layer chromatographic plate affording $[CpWIr_3(\mu\text{-}CO)_3(CO)_6(PPh_3)_2]$ or $[Cp_2W_2Ir_2(\mu\text{-}CO)_3(CO)_6(PPh_3)]$, respectively, but these reactions proceed by the more conventional route of bulky ligand loss and retention of cluster core metals. The conversion of **3** into **4** in the present work must involve break-up of the ditungsten–diiridium core into metal fragments followed by recondensation into the tungsten–triiridium framework of **4**. Kinetic studies on several binuclear and polynuclear compounds have shown that when metal–metal bond fragmentation occurs, complex equilibria can exist between the species of different nuclearity [20]. In the present case, the presence of the bulky ligand at all four cluster vertices is crucial to effect this core transformation.

2.4. NMR studies

The ^{13}C-NMR spectrum of **2** at 320 K reveals one broad signal (200.1 ppm in $CDCl_3$) corresponding to rapid exchange of all ligands. On cooling to 248 K in CD_2Cl_2, one $P(OMe)_3$ signal in the ^{31}P-NMR spectrum and nine carbonyl resonances of equal intensity in the ^{13}C-NMR spectrum (Fig. 4) are resolved, corresponding to the configuration of **2** shown in Fig. 5. We have extended the NMR chemical shift positional sequence established with tetrairidium clusters (bridging > radial > axial ≈ apical [21]) to the mixed-metal regime, affording the chemical shift sequence W–W bridging CO > W–Ir bridging CO > Ir–Ir bridging CO ≈ W terminal CO > Ir radial CO > Ir axial CO ≈ Ir apical CO; it is possible to distinguish Ir–Ir bridging COs from W terminal COs due to the 15% abundant ^{183}W-coupled satellites of the latter [1,8,9]. With this information, it is possible to assign the spectrum of **2**. The presence of at least one carbonyl resonance in the bridging carbonyl region, and only one carbonyl resonance at high field in the apical/axial region of **2** excludes both an all-terminal ligand configuration and the possibility of a W_2Ir basal plane; **2** must therefore have a WIr_2 basal plane. There are two Ir-ligated axial sites, but only one is occupied by carbonyl; the other must therefore be occupied by phosphite. There are six possible configurations which are consistent with this information, corresponding to differing sites for the Cp ligands: the apical Cp ligand can be sited over any of the three non-basal faces, and the basal Cp can be axial or radial. A ^1H-^1H NOESY experiment of **2** in CD_2Cl_2 at 248 K reveals the presence of a crosspeak between the signals at 4.99 and 3.72 ppm, which can be assigned to through

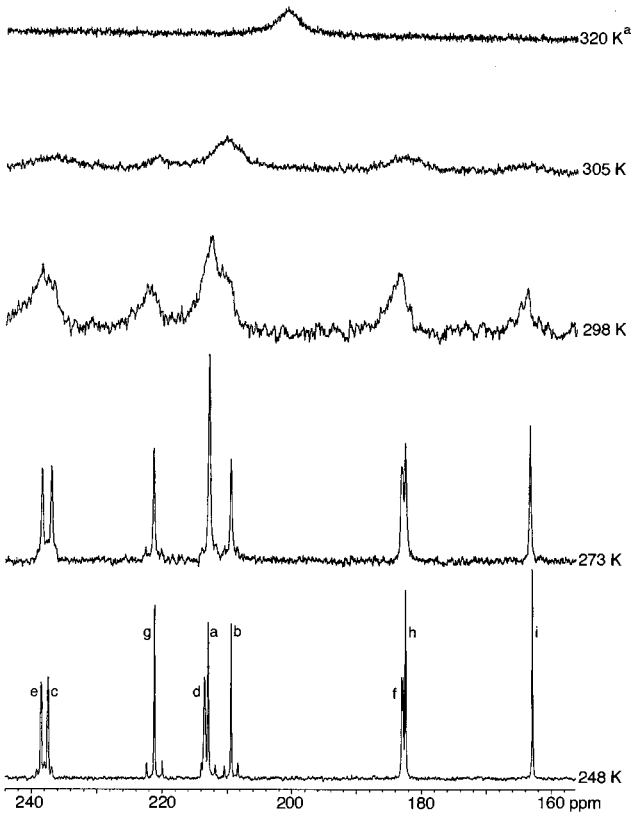

Fig. 4. Variable temperature ^{13}C-NMR spectroscopic study of $[Cp_2W_2Ir_2(\mu\text{-}CO)_3(CO)_6\{P(OMe)_3\}]$ (**2**) in CD_2Cl_2 (a in $CDCl_3$).

space interactions between an axially-disposed Cp and an axially-ligating $P(OMe)_3$, respectively. The chemical shifts of the carbonyl resonances in the ^{13}C-NMR spectrum of **2** are very similar to those reported for $[Cp_2W_2Ir_2(\mu\text{-}CO)_3(CO)_6(PMe_3)]$ [1], strengthening the assignment of a diaxial, apical coordination geometry (it is also significant that this configuration has previously been seen in the structurally characterized $[Cp_2Mo_2Ir_2(\mu\text{-}CO)_3(CO)_6(PMe_3)]$ [22]); all NMR resonances can be assigned analogously to those of $[Cp_2W_2Ir_2(\mu\text{-}CO)_3(CO)_6(PMe_3)]$. ^{183}W-coupled satellites are observed for the resonances at 238.5 (e, 80 Hz), 237.5 (c, 80 Hz), 221.1 (g, 181 Hz), 212.5 (a or b, 154 Hz) and 209.3 ppm (b or a, 156 Hz), corresponding to W–Ir bridging carbonyls, radially ligating W-bound carbonyls and the apical carbonyls. The assignment of carbonyls e and c are confirmed by the presence of a coupling between the axial carbonyl i and the bridging carbonyl c in a ^{13}C-^{13}C correlation spectroscopy (COSY) experiment; a similar (μ-CO)-axial CO coupling has been noted previously in a COSY experiment of $[CpWIr_3(\mu\text{-}CO)_3(CO)_6(PPh_3)]$ [8]. Assignment of the remaining signals in the ^{13}C-NMR spectrum of **2**, namely 213.3 (d), 182.8 [f, $^2J(CP) = 14$ Hz], 182.4 (h) and 162.2 ppm (i), is straightforward because of the *cis* coupling observed at carbonyl f. ^{183}W-coupled satellites are observed in the ^{31}P-NMR spectrum of **2**, in contrast to our previous studies with phosphine-substituted clusters. This result is consistent with an iridium-coordinated $P(OMe)_3$ which ligates axially with respect to the basal plane and is effectively *trans* to the apical tungsten atom (Fig. 5). The ^2J(PW) coupling is possibly due to the fact that Ir–(phosphite) bonds are somewhat shorter than the corresponding Ir–(phosphine) bonds in the related phosphine-substituted tungsten–iridium clusters, but an alternative expanation is that the slow exchange of the ligands surrounding the cluster core (as compared with the related phosphine-substituted derivatives) results in onset of fluxionality at higher temperatures. These higher temperatures afford better resolution for experimental reasons (less viscous solvents, and hence more effective shimming).

Ligand fluxionality commences upon warming the solution. A ^{13}C{^{1}H}-EXSY study at 273 K is shown in Fig. 6. EXSY experiments use a NOESY sequence which allows for a 'mixing time' during which the observed nuclei may migrate to another site. The off-diagonal cross-peaks in the 2D experiment occur between the shifts of exchanging sites [23]. The contour plot for cluster **2** shown in Fig. 6 reveals site exchanges corresponding to h↔b or a, h↔d and b or a↔d. This sequence of carbonyl exchanges has been identified previously in the analogous PMe_3-substituted cluster [24]. Exchanges are consistent with assignment of the signal at 209.3 ppm to carbonyl b, with ligand mobility about the WIr_2 face. The carbonyl distribution in the intermediate is reminiscent of the D_{2d} species implicated in an $[M_4(CO)_{12}]$ exchange pathway [25] (Scheme 1). Carbonyl f is attached to the electron-rich phosphite-ligated iridium and, as previously reported for $[Cp_2W_2Ir_2(\mu\text{-}CO)_3(CO)_6(PMe_3)]$, is expected to have a

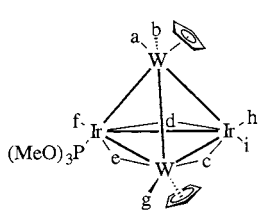

$[Cp_2W_2Ir_2(\mu\text{-}CO)_3(CO)_6\{P(OMe)_3\}]$ (**2**)
axial phosphite, axial Cp, apical Cp

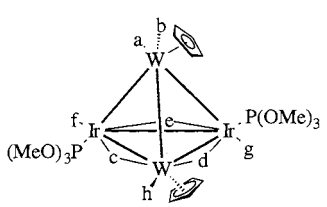

$[Cp_2W_2Ir_2(\mu\text{-}CO)_3(CO)_5\{P(OMe)_3\}_2]$ (**3**)
radial phosphite, axial phosphite, axial Cp, apical Cp

Fig. 5. Configurations of $[Cp_2W_2Ir_2(\mu\text{-}CO)_3(CO)_{7-n}\{P(OMe)_3\}_n]$ ($n = 1$ (**2**) or 2 (**3**)).

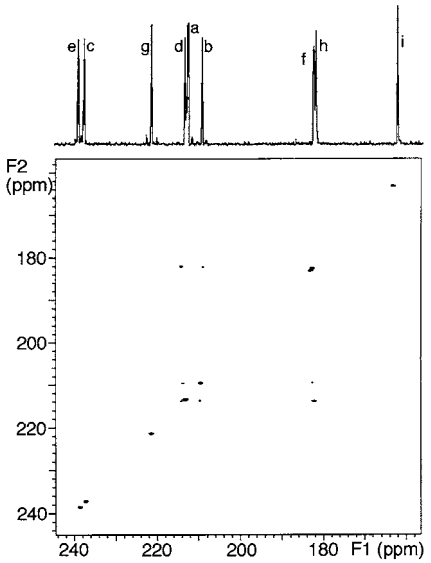

Fig. 6. ^{13}C-NMR EXSY spectrum of $[Cp_2W_2Ir_2(\mu\text{-}CO)_3(CO)_6\{P(OMe)_3\}]$ (**2**) in CD_2Cl_2 at 273 K.

higher activation energy for participation in an exchange of this type.

Unlike other P-substituted derivatives of **1**, the NMR spectra of **3** reveal the carbonyls are undergoing very slow exchange; at r.t., resonances corresponding to the configuration of **3** shown in Fig. 5 can be identified. Raising the temperature results in broadening of the resonances but the coalescence point could not be reached due to slow decomposition of the cluster in solution above 303 K. The carbonyl resonances in the ^{13}C-NMR spectrum of **2** are very similar to those of an isomer of the previously reported $[Cp_2W_2Ir_2(\mu\text{-}CO)_3(CO)_5(PMe_3)_2]$ [1], which was assigned a radial, diaxial, apical configuration with the Cp inclined to a $W_2Ir(P_{rad})$ face, in agreement with the structural characterization of **3**. A ^{1}H-^{1}H NOESY experiment of **3** at 298 K indicates the presence of a crosspeak between the signals at 4.53 and 3.75 ppm, corresponding to through space interactions between the apically-disposed Cp (4.53 ppm) and the radially ligating $P(OMe)_3$ (3.75 ppm). All resonances can therefore be assigned by comparison with the literature data for the trimethylphosphine-containing analogue. ^{183}W-coupled satellites in the ^{13}C-NMR spectrum of **3** are observed for the resonances at 246.0 (c, 70 Hz), 239.0 (d, 80 Hz), 222.7 (h, 185 Hz), 214.2 (a or b, 172 Hz), 212.0 ppm (b or a, 158 Hz), which identifies the W–Ir bridging carbonyls, the radially ligating W-bound carbonyl and the apical carbonyls. Assignment of the remaining signals at 220.5 (e), 185.8 [f, $^2J(CP) = 40$ Hz, $^3J(CP) = 8$ Hz] and 164.3 ppm [g, $^2J(CP) = 42$ Hz] is straightforward due to the *cis* and *trans* coupling observed at carbonyl f, and the *cis* coupling at carbonyl g. ^{183}W-coupled satellites are also observed in the ^{31}P-NMR spectrum of **3**. Both phosphites are effectively *trans* to a tungsten atom; the $^2J(WP)$ coupling not seen in the NMR spectra of related phosphine-substituted clusters is attributed, as above, to the shorter Ir–P bonds in **3**, and the improved resolution of the ^{31}P-NMR spectrum. Ligand fluxionality for **3** commences upon warming the solution, but due to complications arising from the decomposition of **3** to give **4** and other products, we are unable to propose an appropriate exchange mechanism for this cluster.

The geometries adopted by **2** and **3** can be compared with those of related derivatives from the tungsten–triiridium and tetrairidium systems. Trisubstituted derivatives of $[Ir_4(CO)_{12}]$ usually adopt diradial, axial geometries with monodentate ligands (radial, diaxial ligation is preferred with bidentate ligands), whereas trisubstituted derivatives of $[CpWIr_3(CO)_{11}]$ (i.e. bis-phosphine/phosphite derivatives) adopt radial, diaxial or triradial coordination modes [6,8]. Trisubstituted (mono-phosphine) derivatives of $[Cp_2W_2Ir_2(CO)_{10}]$ (**1**) have recently been reported to adopt diaxial, apical coordination geometries ($[Cp_2W_2Ir_2(\mu\text{-}CO)_3(CO)_6(PPh_3)]$, two isomers; $[Cp_2W_2Ir_2(\mu\text{-}CO)_3(CO)_6(PMe_3)]$, one configuration); the coordination geometry and carbonyl exchange pathway proposed for **2** is analogous to that of $[Cp_2W_2Ir_2(\mu\text{-}CO)_3(CO)_6(PMe_3)]$ [1]. Tetrasubstituted derivatives of $[Ir_4(CO)_{12}]$, $[CpWIr_3(CO)_{11}]$ and $[Cp_2W_2Ir_2(CO)_{10}]$ (**1**) most frequently adopt radial, diaxial, apical ligation (with the apical ligand oriented toward the axial substituents) to minimize unfavourable steric interactions. One isomer of $[Cp_2W_2Ir_2(\mu\text{-}CO)_3(CO)_5(PMe_3)_2]$ has also been assigned a radial, diaxial, apical configuration, but with rotation at the tungsten atom, placing the Cp over a radial phosphine-containing W_2Ir face; this configura-

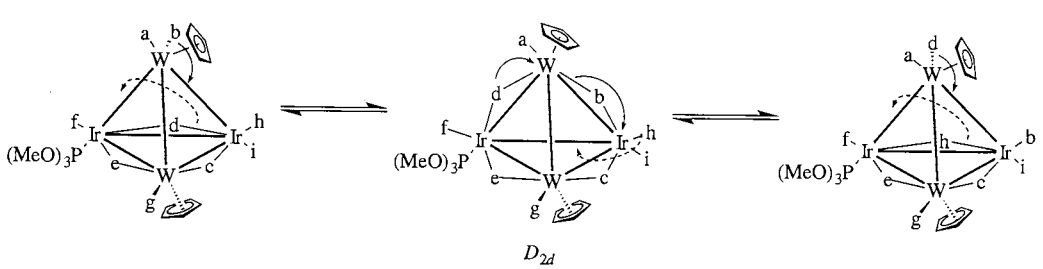

Scheme 1. CO mobility about a WIr_2 face in **2**.

tion is also seen in the current work with $[Cp_2W_2Ir_2(\mu\text{-}CO)_3(CO)_5\{P(OMe)_3\}_2]$, and it seems that this configuration becomes increasingly accessible with small ligands for which steric considerations are less important.

3. Experimental

All reactions were performed under an atmosphere of dry nitrogen (high purity grade, BOC), although no special precautions were taken to exclude air during work-up. The reaction solvent CH_2Cl_2 was dried and distilled from CaH_2 under nitrogen; all other solvents were reagent grade, and used as received. Petroleum ether refers to a fraction of boiling point range 60–80°C. The products of thin-layer chromatography were separated on 20 × 20 cm glass plates coated with Merck GF_{254} silica gel (0.5 mm).

IR spectra were recorded on a Perkin–Elmer system 2000 Fourier transform spectrophotometer with NaCl optics. ^{1}H-, ^{13}C- and ^{31}P-NMR spectra were recorded on a Varian VXR300S spectrometer (^{1}H at 300.0 MHz, ^{13}C at 75.4 MHz and ^{31}P at 121.4 MHz) and are proton decoupled. Spectra were run in $CDCl_3$ (Cambridge Isotope Laboratories) or CD_2Cl_2 (Cambridge Isotope Laboratories); chemical shifts in ppm are referenced to internal residual solvent (^{1}H, $CHCl_3 = 7.24$ ppm; ^{13}C, $CD_2Cl_2 = 53.8$ ppm) or external 85% H_3PO_4 (0.0 ppm). Resonances are reported in the form: ppm (assignment; multiplicity; relative intensity), with the specific assigned sites shown in Fig. 5. The ^{13}C-{^{1}H} EXSY experiments were carried out using the standard NOESY pulse sequence with the mixing time set to 0.05 s. The ^{1}H NOESY experiments were carried out using the standard pulse sequence with the mixing time set to 0.2 s. The integrated ^{13}C-NMR spectra were recorded with a recycle delay of 3–5 times the longest T_1 of the carbonyl ligands. 2D NMR spectra were recorded utilizing a recycle delay of 1–3 times the longest T_1 of the carbonyl ligands. T_1 measurements were carried out employing the standard inversion-recovery procedure.

Mass spectra were obtained at the Australian National University on a VG ZAB 2SEQ instrument (30 kV Cs^+ ions, current 1 mA, accelerating potential 8 kV, matrix 3-nitrobenzyl alcohol). Peaks are reported in the form: m/z (assignment, relative intensity). Elemental microanalyses were performed by the Microanalysis Service Unit in the Research School of Chemistry, Australian National University.

3.1. Reaction of $[Cp_2W_2Ir_2(CO)_{10}]$ with one equivalent of $P(OMe)_3$

A red solution of $[Cp_2W_2Ir_2(CO)_{10}]$ (20.0 mg, 0.0172 mmol) and $P(OMe)_3$ (4.5 mg, 0.0175 mmol) was stirred at r.t. for 16 h. The solution was then evaporated to dryness. The resultant orange residue was dissolved in CH_2Cl_2 (ca. 1 ml) and chromatographed (3 CH_2Cl_2:2 petroleum ether eluant) affording two bands, one in trace amounts. Crystallization of the contents of the first band, R_f 0.60, from CH_2Cl_2/MeOH afforded orange crystals of $[Cp_2W_2Ir_2(\mu\text{-}CO)_3(CO)_6\{P(OMe)_3\}]$ (**2**) (11.9 mg, 54%). Analytical data for **2**: IR (c-C_6H_{12}) 2049w, 2031s, 2007vs, 2004w, 1978s, 1959m, 1922s, 1869m, 1834m cm^{-1}; ^{1}H-NMR ($CDCl_3$, 248 K) δ 4.99 (s, 5H, C_5H_5), 4.68 (s, 5H, C_5H_5), 3.74 [d, $J(PH) = 12$ Hz, 9H, OMe]; ^{13}C-NMR (CD_2Cl_2, 248 K) 238.5 [e, s, 85%, d, 15% $^1J(WC) = 80$ Hz, 1.0], 237.5 [c, s, 85%, d, 15% $^1J(WC) = 80$ Hz, 1.0], 221.1 [g, s, 85%, d, 15% $^1J(WC) = 181$ Hz, 1.0], 213.3 (d, s, 1.0), 212.5 [a, s, 85%, d, 15% $^1J(WC) = 154$ Hz, 1.0], 209.3 [b, s, 85%, d, 15% $^1J(WC) = 156$ Hz, 1.0], 182.8 [f, d, $J(CP) = 14$ Hz, 1.0], 182.4 (h, s, 1.0), 162.8 (i, s, 1.0) ppm; ^{13}C-NMR (CD_2Cl_2, 298 K) 89.2 (s, Cp), 88.6 (s, Cp) ppm; ^{31}P-NMR (CD_2Cl_2, 248 K) 98.8 [s, 85%, d, 15% $^2J(PW) = 43$ Hz, 1P] ppm; MS 1202 ($[M-2CO]^+$, 42), 1174 ($[M-3CO]^+$, 100), 1146 ($[M-4CO]^+$, 79), 1118 ($[M-5CO]^+$, 97), 1090 ($[M-6CO]^+$, 33), 1072 ($[M-7CO]^+$, 30), 1044 ($[M-8CO]^+$, 50), 1016 ($[M-9CO]^+$, 28). Anal. Calc.: C, 21.00; H, 1.52. Found: C, 20.59; H, 1.73%.

3.2. Reaction of $[Cp_2W_2Ir_2(CO)_{10}]$ with two equivalents of $P(OMe)_3$

Following the method of Section 3.1, $[Cp_2W_2Ir_2(CO)_{10}]$ (20.0 mg, 0.0172 mmol) and $P(OMe)_3$ (8.8 mg, 0.0344 mmol) in CH_2Cl_2 (20 ml) afforded two bands after chromatography (3:2 CH_2Cl_2-petroleum ether eluant), one in trace amounts. Crystallization of the contents of the first band, R_f 0.60, from CH_2Cl_2/n-octane afforded orange crystals of $[Cp_2W_2Ir_2(\mu\text{-}CO)_3(CO)_5\{P(OMe)_3\}_2]$ (**3**) (18.1 mg, 76%). Analytical data for **3**: IR (c-C_6H_{12}) 2002vs, 2031s, 1983w, 1949m, 1914s, 1858m, 1807m cm^{-1}; ^{1}H-NMR ($CDCl_3$) δ 4.94 (s, 5H, C_5H_5), 4.53 (s, 5H, C_5H_5), 3.75 [d, $J(PH) = 12$ Hz, 9H, OMe], 3.69 [d, $J(PH) = 12$ Hz, 9H, OMe]; ^{13}C-NMR (CD_2Cl_2, 298 K) 246.0 [c, s, 85%, d, 15% $^1J(WC) = 70$ Hz, 1.0], 239.0 [d, s, 85%, d, 15% $^1J(WC) = 80$ Hz, 1.0], 222.7 [h, s, 85%, d, 15% $^1J(WC) = 185$ Hz, 1.0], 220.5 (e, s, 1.0), 214.2 [a or b, s, 85%, d, 15% $^1J(WC) = 172$ Hz, 1.0], 212.0 [b or a, s, 85%, d, 15% $^1J(WC) = 80$ Hz, 1.0], 185.8 [f, dd, $^2J(CP) = 40$ Hz, $^2J(CP) = 8$ Hz, 1.0], 164.3 [g, d, $^2J(CP) = 8$ Hz, 1.0] ppm; ^{13}C-NMR (CD_2Cl_2, 298 K) 89.5 (s, Cp), 89.3 (s, Cp) ppm; ^{31}P-NMR (CD_2Cl_2, 248 K) 125.3 [s, 85%, d, 15% $^2J(PW) = 42$ Hz, 1P], 99.5 [s, 85%, d, 15% $^2J(PW) = 42$ Hz, 1P] ppm; MS 1298 ($[M-2CO]^+$, 32), 1270 ($[M-3CO]^+$, 100), 1242 ($[M-4CO]^+$, 65), 1214 ($[M-5CO]^+$, 90), 1186 ($[M-6CO]^+$, 23), 1158 ($[M-7CO]^+$, 35). Anal. Calc.: C, 21.28; H, 2.08. Found: C, 21.68; H, 1.98%.

3.3. Structure determinations

Crystals of compound **3**, **4a** and **4b** suitable for diffraction analysis were all obtained by slow evaporation of a solution of **3** in dichloromethane and octane at r.t. Unique diffractometer data sets were measured at ca. 295 K (**3** and **4b**) or ca. 183 K (**4a**) (a unit cell measurement of **4b** at ca. 183 K afforded the same cell parameters as at 295 K) within the specified $2\theta_{max}$ limit ($2\theta/\theta$ scan mode; monochromatic Mo–K_α radiation ($\lambda = 0.7107_3$ Å)), yielding N independent reflections. N_o of these with $I > 3\sigma(I)$ were considered 'observed' and used in the full matrix/large block least squares refinements after empirical absorption correction. Anisotropic thermal parameters were refined for the non-hydrogen atoms; $(x, y, z, U_{iso})_H$ were included, constrained at estimated values. Conventional residuals R, R_w on $|F|$ at convergence are given. Neutral atom complex scattering factors were used, computation using TEXSAN [26]. Pertinent results are given in the figures and tables. Atomic coordinates, bond lengths and angles, and thermal parameters have been deposited at the Cambridge Structural Database.

4. Supplementary material

Crystallographic data for the structural analysis has been deposited with the Cambridge Crystallographic Data Centre. Copies of this material may be obtained free of charge from The Director, CCDC, 12 Union Road, Cambridge, CB2 1EZ, UK (Fax: +44-1223-336-033; e-mail: deposit@ccdc.cam.ac.uk or www: http://www.ccdc.cam.ac.uk).

Acknowledgements

We thank the Australian Research Council for support of this work and Johnson-Matthey Technology Centre for the generous loan of $IrCl_3$. M.G. Humphrey is an ARC Australian Research Fellow.

References

[1] S.M. Waterman, M.G. Humphrey, G.E. Ball, D.C.R. Hockless, Organometallics (1998), submitted for publication.
[2] E.W. Abel, F.G.A. Stone, G. Wilkinson (Eds.), Comprehensive Organometallic Chemistry II, vol. 10, Pergamon Press, Oxford, UK, 1995.
[3] G.F. Stuntz, J.R. Shapley, Inorg. Chem. 15 (1976) 1994.
[4] K. Besançon, G. Laurenczy, T. Lumini, R. Roulet, Helv. Chim. Acta 76 (1993) 2926.
[5] D.J. Darensbourg, B.J. Baldwin-Zuschke, J. Am. Chem. Soc. 104 (1982) 3906.
[6] S.M. Waterman, M.G. Humphrey, D.C.R. Hockless, J. Organomet. Chem. 555 (1998) 25.
[7] S.M. Waterman, M.G. Humphrey, D.C.R. Hockless, J. Organomet. Chem. (1998), in press.
[8] S.M. Waterman, M.G. Humphrey, Organometallics 579 (1999) 75.
[9] S.M. Waterman, M.G. Humphrey, D.C.R. Hockless, J. Organomet. Chem. 565 (1998) 81.
[10] S.M. Waterman, M.G. Humphrey, V.-A. Tolhurst, B.W. Skelton, A.H. White, Organometallics 15 (1996) 934.
[11] M.R. Churchill, C. Bueno, J.P. Hutchinson, Inorg. Chem. 21 (1982) 1359.
[12] M.R. Churchill, J.P. Hutchinson, Inorg. Chem. 20 (1981) 4112.
[13] G. Ciani, M. Manassero, V.G. Albano, F. Canziani, G. Giordano, S. Martinengo, P. Chini, J. Organomet. Chem. 150 (1978) C17.
[14] G. Bondietti, R. Ros, R. Roulet, F. Musso, G. Gervasio, Inorg. Chim. Acta 213 (1993) 301.
[15] F. Ragaini, F. Porta, F. Demartin, Organometallics 10 (1991) 185.
[16] D.J. Darensbourg, M.J. Incorvia, Inorg. Chem. 20 (1981) 1911.
[17] E. Iiskola, T. Pakkanen, Acta Chem. Scand. A 38 (1984) 731.
[18] J. Pursiainen, T.A. Pakkanen, J. Jääskeläinen, J. Organomet. Chem. 290 (1985) 85.
[19] J. Pursiainen, M. Ahlgren, T. Pakkanen, J. Valkonen, J. Chem. Soc. Dalton Trans. (1990) 1147.
[20] A. Pöe, Chem. Br. 19 (1983) 997.
[21] R. Ros, A. Scrivanti, V.G. Albano, D. Braga, J. Chem. Soc. Dalton Trans. (1986) 2411.
[22] N.T. Lucas, M.G. Humphrey, P.C. Healy, M.L. Williams, J. Organomet. Chem. 545 (1997) 519.
[23] A.E. Derome, Modern NMR Techniques for Chemistry Research, Pergamon Press, Oxford, 1987.
[24] S.M. Waterman, M.G. Humphrey, unpublished results.
[25] E. Band, E.L. Muetterties, Chem. Rev. 78 (1978) 639.
[26] TEXSAN, Single-crystal Structure Analysis Software, Version 1.7-3, Molecular Structure Corporation, The Woodlands, TX, USA, 1995.